Assessing Synergistic Ultrafiltration Membrane Fouling by TiO$_2$ Nanoparticles and Humic Acid Using Interaction Energy Analysis

Lin Tian[1], Chunyi Sun[1], Fengkai Sun[2], RuiQiang Zong[3], Shuang Liang[1*]

[1]Shandong Provincial Key Laboratory of Water Pollution Control and Resource Reuse, School of Environmental Science and Engineering, Shandong University, Jinan 250100, China
[2]Shandong Daojian Environmental Protection Technology Co., Ltd. Jinan 250014, China
[3]Department of Environmental Engineering, Texas A&M University, Kingsville 700 University Boulevard, Kingsville, TX 78363-8202, USA

Abstract

This research attempts to elucidate the effect of humic acid (HA) on TiO$_2$ nanoparticle ultrafiltration (UF) membrane fouling, and quantitatively analyze the synergistic membrane fouling mechanisms using interaction energies. The extended Derjaguin-Landau-Verwey-Overbeek (xDLVO) theory was employed to analyze the interaction energies and predict UF membrane fouling. Membrane fouling effects were studied during the dead-end filtration of individual TiO$_2$ and HA-TiO$_2$ mixtures using two kinds of polymeric UF membranes. It was found that HA-TiO$_2$ mixtures lead to greater flux declines than individual TiO$_2$. For specific foulant, the hydrophobic PVDF membrane showed relative severe membrane fouling than hydrophilic PES membrane. As for the HA-TiO$_2$ mixture, much higher irreversible fouling was observed compared with that of individual TiO$_2$. Moreover, this study highlights the importance of HA concentration in synergistic fouling effects of the HA-TiO$_2$ mixture. The increase of HA concentration caused an increase of contact angle and lower interaction energy, thus aggravating membrane fouling. Results illustrated that synergistic membrane fouling by TiO$_2$ and HA could be successfully explained using the xDLVO analysis. The extent of membrane fouling turned out to be dominated by Lewis acid-base interaction.

Introduction

Recently, engineered nanoparticles have been widely used in numerous industrial products, resulting in an increasing discharge of nanoparticles into aquatic systems [1-2]. Engineered nanoparticles have been observed to be toxic to microbes, plants, animals, and ecosystems [3]. As a result, engineered nanoparticles represent an emerging category of foulants. More attention has been paid to how engineered nanoparticles will be removed by – and impact the performance of – wastewater treatment systems [4]. Ultrafiltration (UF) has been acknowledged as a promising technology for removing nanoparticles due to its high-quality effluent, reliability in operation,

---

*e-mail: liangshuang@sdu.edu.cn

and small footprint [5-6]. However, membrane fouling remains a major obstacle for the widespread application of ultrafiltration, resulting in severe flux decline, reduced performance, and frequent membrane cleaning.

As an important emerging membrane foulant, the fouling behaviors of nanoparticles have attracted great attentions in recent years [7-10]. However, these studies on membrane fouling behaviors were merely worked with individual nanoparticles. In practice, more than one type of foulant co-exists, and apparently the complex fouling phenomenon cannot be fully understood by studying nanoparticles without other foulants.

Natural organic matter (NOM) is ubiquitous in nearly all aquatic environments. Once released into the environment, nanoparticles can adsorb NOM to form complexes [11]. It is generally known that the adsorption of NOM modifies the surface properties of nanoparticles [12-13]. Therefore, the presence of NOM is expected to influence the membrane fouling mechanism. Earlier studies have observed a synergistic effect between NOM and common inorganic colloids on membrane fouling [14-16]. Jermann et al. [15] found a significant stronger flux decline during the filtration of mixed solutions consisting of humic acid and kaolinite particles, in comparison with individual foulants. Compared with common inorganic particles, the high surface-area-to-volume ratio makes the behavior of nanoparticles during membrane filtration significantly different. As a consequence, the knowledge of NOM-colloid cannot be completely applicable to NOM-nanoparticle. However, to our best knowledge the synergistic fouling effect of nanoparticles and NOM has not been purely understood.

Interactions assessment during filtration is significant to further understand membrane fouling. Therefore, a quantitative interfacial interaction analysis for understanding the fouling mechanism of nanoparticles in the presence of NOM needs to be studied. Recently, the extended Derjaguin-Landau-Verwey-Overbeek (xDLVO) theory has been successfully used to predict membrane fouling and analyze the fouling mechanism quantitatively [10, 17]. It is the summation of the Lifshitz/van der Waals interactions (LW), the electrical double-layer interactions (EL), and the Lewis acid-base interactions (AB). According to xDLVO theory, LW as well as AB interactions are also considered to contribute to membrane fouling mechanisms, and the effect of EL interaction is not a key factor influencing the total interaction. However, substantial efforts have been spent on the influence of electrostatic interactions during nanoparticle membrane fouling [7, 10-11]. Not much is known on the fouling mechanism of nanoparticles in the presence of NOM and whether the xDLVO approach is feasible to predict their membrane fouling.

In this study, ultrafiltration experiments and xDLVO theory were applied in order to examine the combined membrane fouling mechanism of nanoparticles and NOM. Among engineered nanoparticles, titanium dioxide (TiO$_2$) is one of the most extensively applied nanoparticles and may occur at the highest concentration [18]. TiO$_2$ and humic acid (HA) were employed in the experiment as representatives of nanoparticles and NOM, respectively. The present work is focused on the effect of the HA concentration on synergistic UF fouling, and on the possible description by the xDLVO theory. The results may allow for a further understanding of the synergistic fouling effect of nanoparticles and NOM on UF membrane.

Experimental

Model Foulants and Membranes

TiO$_2$ nanoparticles employed in this study were P25 Evonik Degussa, with a phase composition of 18% rutile and 82% anatase. According to the manufacturer, this TiO$_2$ has a purity of 99.5% and a primary particle size of 21 nm. The stock suspensions (1 g/L) were prepared by adding TiO$_2$ powders into deionized (DI) water, and followed by sonicating for 15 min (200 W/L and 50 KHz) using a sonication bath. HA supplied by Sigma Aldrich was selected as the representative of NOM substances. The stock HA solution of 1 g/L was prepared by dispersing the powdered HA in DI water and followed by filtration using a 0.45 μm nylon membrane to remove insoluble substances. To investigate the effect of HA concentration on membrane fouling of the HA-TiO$_2$ mixture, five HA-TiO$_2$ mixture samples containing HA concentrations of 0, 2, 3, 5, and 10 mg/L were prepared. The final concentration of TiO$_2$ in all five water samples was 10 mg/L. The pH was adjusted to 7.5 with 0.1 M HCl and 0.1 M NaOH. The ionic strength was 10 mM by the addition of 0.1 M NaCl in all experiments.

Two kinds of 100 kDa ultrafiltration membranes (Shanghaimosu Filtering Equipment Co. Ltd., Shanghai, China) made of polyethersulfone (PES) and polyvinylidene fluoride (PVDF) were employed for each experiment. PES membrane is a relatively hydrophilic membrane (water contact angle 43.6°±1.5°) and is negatively charged (= -30.27 mV); PVDF membrane is a relatively hydrophobic membrane (water contact angle 83.0°±2.9°) and the charge is about -24.57 mV. The PVDF membrane was immersed in 75% (v/v) alcohol for about 2 h to ensure the membrane was sufficiently wetted and degassed [19]. Before use, the two kinds of membrane were first soaked in DI water for 24 h, and then rinsed by filtering at least 2 L of pure water filtration at the pressure of 100 kPa to remove the impurities on membranes.

Physicochemical Characterization

Contact angle measurement was performed using the sessile drop method with a goniometer (JC2000C Contact Angle Meter, Shanghai Zhongchen Experiment Equipment Co. Ltd., China), an instrument that has image analysis attachments, including video camera, monitor and image-analysis software. Three kinds of probe liquids selected for contact angle measurement were DI water, glycerol, and diiodomethane.

Zeta potential and average size were determined using a streaming potential the DelsaNano C (Beckman Coulter, Germany) with dynamic light scattering (DLS) and a Zeta potential device. Each data value is an average of five measurements. All the measurements were performed at room temperature (20ºC).

Surface Tension Parameters Analysis

Surface tension parameters (γ^{LW}, γ^+, and γ^-) of membranes and foulants were determined by performing contact angle measurements and employing extended Young's equation [20].

$$(1+\cos\theta)\gamma_l^{TOT} = 2(\sqrt{\gamma_s^{LW}\gamma_l^{LW}} + \sqrt{\gamma_s^+\gamma_l^-} + \sqrt{\gamma_s^-\gamma_l^+})$$

(1a)

$$\gamma^{TOT} = \gamma^{LW} + \gamma^{AB}$$

(1b)

$$\gamma^{AB} = 2\sqrt{\gamma^+\gamma^-}$$

(1c)

...where θ is the contact angle and γ^{TOT} is total surface tension, which is the sum of LW (apolar) and AB (polar) components, γ^{LW} is the LW component, γ^+ is the electron acceptor parameter, and γ^- is the electron donor parameter. The subscripts s and l correspond to the solid surface and the liquid, respectively. The surface tension components of solid surface (γ_s^{LW}, γ_s^+, and γ_s^-) can be calculated according to contact angle measured using three probe liquids with known surface tension parameters (γ_l^{LW}, γ_l^+, and γ_l^-). The surface tension parameters of the probe liquids are given in Table 1.

Surface tensions (γ^{LW}, γ^+, γ^-) can be employed to calculate the free energy per unit area. The free energy per unit area signifies the interaction energy when the separation between two surfaces is close to the minimum equilibrium cutoff distance (0.158 nm), which was determined from the sum of LW and AB components. The LW and AB free energy per unit as expressed by Eq. (2a) and Eq. (2b) are:

$$\Delta G_{d_0}^{LW} = 2(\sqrt{\gamma_3^{LW}} - \sqrt{\gamma_1^{LW}})(\sqrt{\gamma_2^{LW}} - \sqrt{\gamma_3^{LW}})$$

(2a)

$$\Delta G_{d_0}^{AB} = 2\sqrt{\gamma_3^+}(\sqrt{\gamma_1^-} + \sqrt{\gamma_2^-} - \sqrt{\gamma_3^-}) + 2\sqrt{\gamma_3^-}(\sqrt{\gamma_1^+} + \sqrt{\gamma_2^+} - \sqrt{\gamma_3^+}) - 2(\sqrt{\gamma_1^+\gamma_2^-} + \sqrt{\gamma_1^-\gamma_2^+})$$

(2b)

If surfaces 1 and 2 are different materials (e.g., foulant and membrane), then the sum is the free energy of adhesion; $\Delta G_{d_0}^{LW}$ is the LW adhesion energy and $\Delta G_{d_0}^{AB}$ is the AB adhesion energy. If the two surfaces are composed of identical materials (e.g., two identical foulants), then the sum is the free energy of cohesion $\Delta G_{d_0}^{CO}$. The free energy

Table 1. Surface tension parameters (mJ/m^2) of the liquids used for contact angle measurement (20ºC).

Probe liquids	γ^{LW}	γ^+	γ^-	γ^{TOT}
DI water	21.8	25.5	25.5	72.8
Glycerol	34.0	3.9	57.4	64.0
Diiodomethane	50.8	0.0	0.0	50.8

of cohesion offers insight into foulant stability as well as foulant deposition onto surfaces already covered by the same foulants.

Interaction Energy Analysis Using xDLVO Theory

Total interaction energy was determined from the sum of the Lifshitz-Van Der Waals (LW) and acid-base (AB) and electrostatic (EL) interactions, which can be written as:

$$U^{TOT} = U^{LW} + U^{AB} + U^{EL}$$

(4)

Each component of xDLVO interaction energies was obtained using LW-AB-EL relationship from surface tensions and zeta potential data that were measured experimentally [20].

$$U_{mlf}^{LW}(d) = -\frac{A}{12\pi d^2}$$

(5a)

$$U_{mlf}^{AB}(d) = \Delta G_{d_0}^{AB} \exp(\frac{d_0 - d}{\lambda})$$

(5b)

$$U_{mlf}^{EL}(d) = \varepsilon_r\varepsilon_0\kappa\zeta_m\zeta_f\left(\frac{\zeta_m^2 + \zeta_f^2}{2\zeta_m\zeta_f}(1 - \coth\kappa d) + \frac{1}{\sin\kappa d}\right)$$

(5c)

...where A ($= -12\pi d_0^2\Delta G_{d_0}^{LW}$) is the Hamaker constant, d is the separation distance between the flat plate (membrane) and the sphere (foulant), d_0 (0.158±0.009 nm) is the minimum equilibrium cut-off distance, λ (0.6nm) is the characteristic decay length of AB interaction in water, $\varepsilon_r\varepsilon_0$ (6.95×10^{-10} C^2 J^{-1} m^{-1}) is the dielectric per-mittivity of water, κ (0.104 nm^{-1}) is the inverse Debye screening length, ζ_m and ζ_f are the zeta potentials of membrane and foulant, $\Delta G_{d_0}^{LW}$ is the LW adhesion energy per unit, and $\Delta G_{d_0}^{AB}$ is the AB adhesion energy per unit.

Ultrafiltration Experiments

The dead-end ultrafiltration was conducted using a stirred cell operated at room temperature. The stirred

cell has an inner diameter of 8 cm providing an effective filtration area of 50.26 cm² with an effective volume of 300 mL, which was connected to a steel reservoir with a volume of 10 L. To avoid any possible automatic settling of the foulants, continuous stirring at a speed of 180 rpm was conducted throughout the experiments. The trans-membrane pressure was maintained at 100 kPa, which was provided by a nitrogen gas cylinder.

Before each run of experiments, DI water was filtered through the membrane prior to the fouling experiment to stabilize the filtration system and flush the impurities in the membrane pore. When stable flux was achieved, the initial DI flux J_0 was then measured. Then feed solution was introduced into the stirred-cell, and filtration was stopped when permeate flux leveled off. After the flux in the end of filtration (J_e) was obtained, the fouled membranes were back-washed with DI applying a pressure of 100 kPa on the permeate side. Once the backwash was finished, DI was filtered to determine the water flux J_W after the backwash. To describe the reversible and irreversible fouling in the filtration, the fouling indicators were calculated according to:

$$TF = IF + RF = \frac{J_0 - J_e}{J_0} = 1 - \frac{J_e}{J_0} \tag{6a}$$

$$IF = \frac{J_0 - J_W}{J_0} = 1 - \frac{J_W}{J_0} \tag{6b}$$

…where J_0 is the flux at the start of the experiment, J is permeate flux at given filtration time, and J_W is water flux after backwash. Total fouling (TF) was quantified according to the difference between the flux J_e in the end of filtration and the initial flux J_0. TF is the sum of irreversible (IF) and reversible fouling (RF).
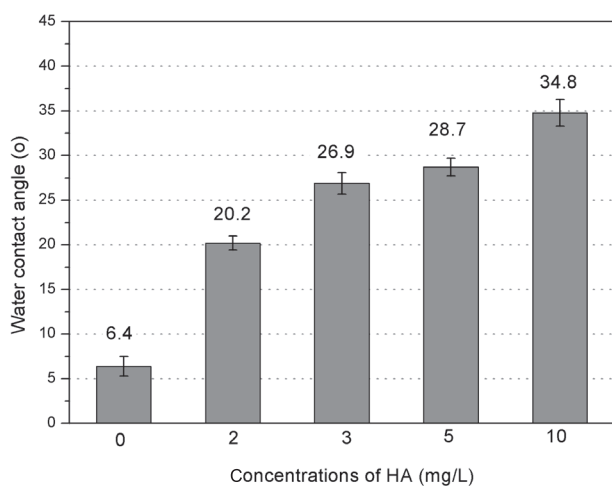
Results and Discussion

Physicochemical Characterization of Model Foulants

Water contact angle (θ_w) of foulant usually can be a reliable indicator for its hydrophilic/hydrophobic property that is fundamentally linked with its surface functional groups. In Fig. 1, contact angles of TiO$_2$ nanoparticles mixed with various concentrations of HA are plotted. The water contact angle (θ_w) of TiO$_2$ was determined to be merely 6.4°, which provides the quantitative evaluation of its extremely hydrophilic nature. The result is consistent with the fact that TiO$_2$ has a large amount of hydroxyl groups [12], resulting in interacting favorably with water. Water contact angles of HA-TiO$_2$ mixture with various HA concentrations were in the 20~35° range, which has not been investigated. This indicates that the addition of HA led to an increase in the contact angle of TiO$_2$ in water and made the HA-TiO$_2$ mixture more hydrophobic. HA carries many functional groups, such as carboxylic (–COOH) and phenolic (–OH). These highly reactive polar groups tend to bound with hydroxyl groups on TiO$_2$ surfaces [12], which can provide less hydroxyl groups and minimize contact with water molecules.

Regarding zeta potentials, it can be seen from Fig. 2 that the zeta potential values of TiO$_2$ gradually decreased with increasing HA concentration. This indicates that HA adsorption could dominate the surface charges of the HA-TiO$_2$ mixture and cause the HA-TiO$_2$ mixture to be highly negatively charged. A decrease of hydroxyl groups for protonation after HA adsorption could be partly responsible for the decrease in zeta potential. Compared with TiO$_2$ in the absence of HA, the HA-TiO$_2$ mixture could be more stable in water, which was evidenced by the hydrodynamic sizes. The average value of hydrodynamic size for individual TiO$_2$ was higher than that of the HA-TiO$_2$ mixture, and decreased when the HA concentration increased. This is consistent with the analysis on the

Fig. 1. Contact angles of TiO$_2$ nanoparticles with various concentrations of HA.
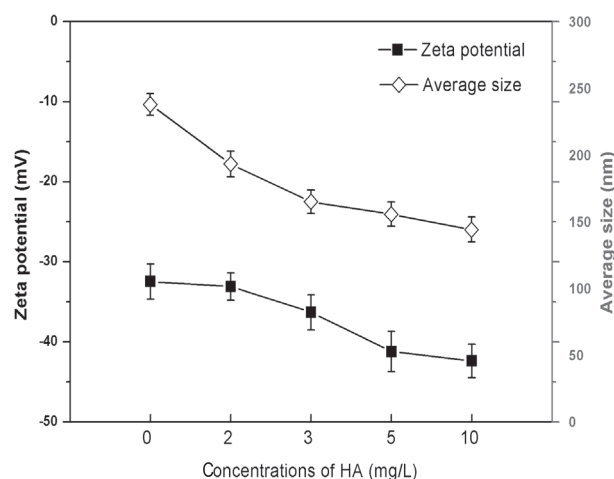
Fig. 2. Zeta potential and average size of TiO$_2$ nanoparticles with various concentrations of HA.

effect of HA adsorption on surface charge status of TiO_2. It was reported earlier that HA addition brought greater electronegativity to the TiO_2 surface, therefore resulting in stronger electrostatic repulsion and more stable suspensions [7].

Surface Tension Parameters and Free Energy of Cohesion

Table 2 lists the surface tension parameters of membranes and TiO_2 nanoparticles mixed with various concentrations of HA. It could be observed that the two membranes made from different polymer material featured different polar and apolar characteristics. PVDF membrane had the higher γ^{LW}, meaning that PVDF membrane presented more apolar properties than the PES membrane. As can be obtained from the values of γ^-, both membranes possessed larger γ^- compared with γ^+, suggesting that they have more electron donor functional groups. Furthermore, the γ^- parameter of PVDF membrane is significantly smaller than that of PES membrane. It could be also found that all the foulants exhibited high electron donor components (γ^-) and relatively low electron acceptor components (γ^+), which was likely to lead to a low acid-base surface tension (γ^{AB}). In addition, total surface tension (γ^{TOT}) of the HA-TiO_2 mixture turned out to be smaller than that of individual TiO_2, which originated from lower values of γ^{AB}. Because the zeta potential and contact angle of the HA-TiO_2 mixture were altered with the increasing concentration of HA, the surface tension parameters could change as well. It was observed that both γ^- and γ^+ of the HA-TiO_2 mixture decreased at higher HA concentration. In contrast, the change tendency of γ^{LW} with increasing HA concentration was irregular. Additionally, there was higher γ^-/γ^+ as the content of HA increased, which may be due to the increased level of deprotonation [21]. Increasing γ^-/γ^+ functionality probably due to HA had a "charging-up" effect on TiO_2. HA absorption on TiO_2 surfaces would lead to the dissociation of –COOH and phenolic –OH groups, which could give rise to easier deprotonation.

The free energy of cohesion $\Delta G_{d_0}^{CO}$ represents the free energy (per unit area) when two surfaces of the same material are immersed in water and brought into contact [22]. The negative $\Delta G_{d_0}^{CO}$ suggests hydrophobic (attractive to each other) and thermodynamically unstable states, while positive $\Delta G_{d_0}^{CO}$ suggests hydrophilic (repulsive to each other) and stable states. Hence, it could be concluded from Table 2 that PES membrane and foulants were hydrophilic. The negative value for PVDF membrane suggested it was hydrophobic. Notably, the calculated free energy of cohesion of HA-TiO_2 became significantly lower with the increase of HA concentration. This indicates that HA could disperse the TiO_2 nanoparticles to some degree in water and enhance hydrophobicity of TiO_2, which was also verified in the contact angle data. When in contact with the fouled membrane surface, the more hydrophobic HA-TiO_2 mixture can exhibit a stronger attractive effect compared with TiO_2, resulting in a higher level of membrane fouling.

Interaction Energy Analysis

Table 3 shows the calculated LW, AB, EL, and total interaction energy between each foulant and membrane. According to xDLVO theory, a positive value of interactive energy between membrane and foulant represents resistance to membrane fouling, while a negative value represents an attractive effect that would aggravate membrane fouling [20]. As shown in Table 3, all the total interaction energies between PES membrane and foulants were positive, whereas the total interaction energies between PVDF membrane and foulants exhibited negative. This indicates that PVDF membrane maybe suffered relatively more severe fouling than PES membrane. In other words, the strongest attractive interaction would occur between PVDF membrane and foulants.

Table 2. Surface tension parameters and free energy of cohesion (mJ/m²) of membranes and TiO_2 nanoparticles with various concentrations of HA.

Materials	γ^{LW}	γ^-	γ^+	γ^-/γ^+	γ^{AB}	γ^{TOT}	$\Delta G_{d_0}^{CO}$
Membranes							
PES	34.56	40.40	0.41	8.15	42.71	98.54	20.11
PVDF	37.55	2.79	0.76	2.77	40.32	3.67	-60.73
Foulants							
TiO_2	49.87	45.14	1.64	27.52	17.21	67.08	13.71
TiO_2 + 2 mg/L HA	49.97	42.74	0.93	45.96	12.61	62.58	12.79
TiO_2 + 3 mg/L HA	49.35	40.23	0.71	56.66	10.69	60.04	10.66
TiO_2 + 5 mg/L HA	48.90	39.56	0.60	65.93	9.74	58.64	10.40
TiO_2 + 10 mg/L HA	48.83	36.40	0.42	86.67	7.82	56.65	6.56

Table 3. Interaction energy (mJ/m²) between foulants and membranes.

PES membrane-foulant	$U_{mlf}^{LW}(d_0)$	$U_{mlf}^{AB}(d_0)$	$U_{mlf}^{EL}(d_0)$	$U_{mlf}^{xDLVO}(d_0)$
TiO$_2$	-5.79	24.52	0.21	18.94
TiO$_2$ + 2 mg/L HA	-5.81	23.75	0.21	18.15
TiO$_2$ + 3 mg/L HA	-5.70	22.35	0.17	16.82
TiO$_2$ + 5 mg/L HA	-5.62	22.06	0.03	16.47
TiO$_2$ + 10 mg/L HA	-5.61	20.13	-0.02	14.50
PVDF membrane-foulant	$U_{mlf}^{LW}(d_0)$	$U_{mlf}^{AB}(d_0)$	$U_{mlf}^{EL}(d_0)$	$U_{mlf}^{xDLVO}(d_0)$
TiO$_2$	-6.98	-11.53	0.05	-18.46
TiO$_2$ + 2 mg/L HA	-7.00	-15.18	0.03	-22.15
TiO$_2$ + 3 mg/L HA	-6.87	-17.63	-0.09	-24.59
TiO$_2$ + 5 mg/L HA	-6.78	-18.53	-0.36	-25.67
TiO$_2$ + 10 mg/L HA	-6.77	-21.53	-0.44	-28.74

The composition of interaction energy clearly showed that LW interaction energy between different membranes and foulants were negative, which means LW interaction energy had an effect of facilitating PES and PVDF membrane fouling. Notably, AB interaction energies between PES membrane and foulants were positive. This indicates that the foulant approaching PES membrane surface not only experienced an attractive energy, but also needed to overcome repulsive interaction energy. In contrast, AB interaction energies between PVDF membrane and foulants were negative, which implies that AB interaction could aggravate PVDF membrane fouling. EL interaction energy had less influence on the composition of total interaction energy, which is consistent with another study [17]. It can thus be concluded that AB interaction energy played a more important role than LW and EL interaction energy at short distances. The AB interaction energy determined the adhesion process of foulants onto the membrane surface and thus influenced the extent of membrane fouling.

The hydrophilic or hydrophobic properties of surfaces can be derived from AB interaction energies. Surfaces with positive AB interaction energies are termed hydrophilic, as foulant-water interactions are favored over polar foulant-foulant interactions. It was observed that AB interaction energy of HA-TiO$_2$ mixture decreased with increasing HA content, which is in accordance with the variation tendency of $\Delta G_{d_0}^{CO}$. Owing to the dominant role of AB interaction energy, total interaction energies also had a similar tendency. TiO$_2$ in the absence of HA is considered relatively less fouling with the both membrane than the HA-TiO$_2$ mixture. Additionally, for both PES and PVDF membranes, the total interaction energies were decreased with an increase of HA concentration, which could cause more severe membrane fouling. The total interaction energies between the membrane and TiO$_2$ in the presence of 10 mg/L HA approached the lowest value, indicating the highest level of membrane fouling.

Filtration Behavior

To verify the interaction energy predictions, the flux decline and fouling reversibility of membranes for individual and premixed foulants were studied. The flux decline trends of two membranes for individual TiO$_2$ nanoparticles and HA-TiO$_2$ mixtures are shown in Fig. 3. Comparing the flux reduction of foulants with PES membrane to that with PVDF membrane, it can be concluded that foulants are favorable for depositing on PVDF membrane, which accords with the xDLVO predictions. The total interaction energies between PES membrane and foulants were strongly repulsive, but all the total interactions between PVDF membrane and foulants systems were attractive. Therefore, for a specific foulant, the hydrophobic PVDF membrane would suffer more severe fouling than the hydrophilic PES membrane.

For both PVDF and PES membranes, the fouling propensity of foulants was in the same order. It can be observed that individual TiO$_2$ causes only a minor flux decline. The minor reduction in normalized flux of nanoparticles without an organic background is in agreement with results from Springer et al. [23], Jermann et al. [24], and Tian et al. [25]. However, the mixtures of TiO$_2$ and HA lead to greater flux decreases than that of the individually filtered TiO$_2$. Additionally, the flux decline of HA-TiO$_2$ mixtures became faster with an increase of the HA concentration, which corresponded to the calculated interaction energy. A lower interaction energy would therefore result in an aggravation of membrane fouling. Based on xDLVO predictions, TiO$_2$ in the presence of 10 mg/L HA exhibited the lowest interaction energy, indicating the greatest membrane fouling. The results
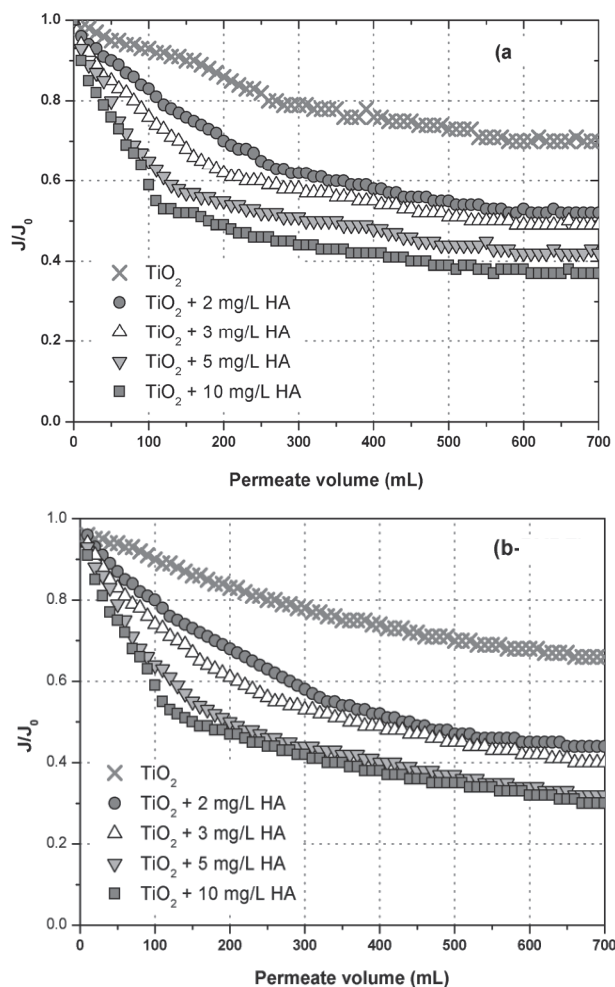
Fig. 3. Flux decline profiles of a) PES and b) PVDF membranes for individual TiO$_2$ and HA-TiO$_2$ mixtures.

Fig. 4. Relative fouling of (a) PES and (b) PVDF membranes for individual TiO$_2$ and HA-TiO$_2$ mixtures.

indicate that the membrane fouling was significantly influenced by the HA concentration, and fouling potential could be explained by the xDLVO theory.

The irreversible and reversible fouling values in the entire filtration process are shown in Fig. 4. Higher irreversible fouling (IF) indicates that only a small part of the overall filtration resistance can be removed by back-washing [24]. As could been seen, the irreversible fouling (IF) of the PVDF membrane was higher than that of the PES membrane. Because the total interaction energies of PVDF membrane-foulant interactions were negative and PES membrane-foulant interactions were positive, it is difficult to remove foulants from PVDF membrane surface by back-washing, which gives rise to the much higher IF than PES membrane. Individual TiO$_2$ nanoparticles showed a relatively higher reversible fouling (RF) than irreversible fouling (IF). However, when the HA was added, synergistic fouling effect was observed between HA and TiO$_2$ nanoparticles, as evidenced by a considerably greater irreversible fouling. Additionally, the increase trend of the IF at higher HA concentration could also be observed, indicating that HA plays a critical role in synergistic irreversible fouling effect

of the HA-TiO$_2$ mixture. Because the interaction energies become lower with increasing HA concentration, the foulants are removed more uneasily from the membrane surface at higher HA concentration. This implied that the irreversible fouling is mainly linked with interaction energies between membranes and foulants. In contrast, with the increase of HA concentration from 2 mg/L to 10 mg/L, only a little change in reversible fouling (RF) was observed.

Conclusions

The results provide evidence for a synergistic membrane fouling effect of HA and TiO$_2$ nanoparticles during ultrafiltration. The fouling mechanism of HA-TiO$_2$ mixture was determined by interaction energies, and fouling potential could be well explained by the xDLVO theory. The AB interfacial interaction played a dominant role in three interfacial interactions. It has been found that HA absorption can influence the properties of TiO$_2$ nanoparticles. As a result, HA-TiO$_2$ mixtures lead to greater flux decreases than that of individual TiO$_2$, and the flux decline became greater

with an increase of HA concentration. Membrane fouling experiments had been performed using two commercial polymeric UF membranes. It was shown that the fouling severity of PVDF membrane was higher than that of the PES membrane, which was consist with the predictions of the xDLVO approach.

Our study results may improve predictions of UF membrane fouling by nanoparticles in natural waters. Further studies on NOM-nanoparticle interactions using various kinds of nanoparticles and NOM may be conducted to extend the knowledge on the role of NOM-nanoparticle interactions in UF fouling.

Acknowledgements

References

1. LIU H.H., COHEN Y. Multimedia environmental distribution of engineered nanomaterials. Environmental science & technology. **48** (6), 3281, **2014**.

2. HEGDE K., BRAR S.K., VERMA M. Current understandings of toxicity, risks and regulations of engineered nanoparticles with respect to environmental microorganisms. Nanotechnology for Environmental Engineering. **1** (1), 5, **2016**.

3. KOWALSKA-GÓRALSKA M., SENZE M. Biocidal properties of silver-nanoparticles in water environments. Polish Journal of Environmental Studies. **24** (4), 1641, **2015**.

4. VON MOOS.N., SLAVEYKOVA V.I. Oxidative stress induced by inorganic nanoparticles in bacteria and aquatic microalgae-state of the art and knowledge gaps. Nanotoxicology. **8** (6), 605, **2014**.

5. GUO H., WYART Y., PEROT J. Low-pressure membrane integrity tests for drinking water treatment: A review. Water research. **44** (1), 41, **2010**.

6. SPRINGER F., LABORIE S., GUIGUI C. Removal of SiO_2 nanoparticles from industry wastewaters and subsurface waters by ultrafiltration: investigation of process efficiency, deposit properties and fouling mechanism. Separation and Purification Technology. **108**, 6, **2013**.

7. TRZASKUS K.W. Towards controlled fouling and rejection in dead-end microfiltration of nanoparticles-Role of electrostatic interactions. Journal of membrane science. **496**, 174, **2015**.

8. SINGH G., SONG L. Experimental correlations of pH and ionic strength effects on the colloidal fouling potential of silica nanoparticles in crossflow ultrafiltration. Journal of Membrane Science. **303** (1), 112, **2007**.

9. YIN T., WALKER H.W., CHEN D. Influence of pH and ionic strength on the deposition of silver nanoparticles on microfiltration membranes. Journal of Membrane Science. **449**, 9, **2014**.

10. HENRY C., BRANT J.A. Mechanistic analysis of microfiltration membrane fouling by buckminsterfullerene (C 60) nanoparticles. Journal of membrane science. **415**, 546, **2012**.

11. HENRY C., DORR B., BRANT J.A. Buckminsterfullerene (C 60) nanoparticle fouling of microfiltration membranes operated in a cross-flow configuration. Separation and purification technology. **100**, 30, **2012**.

12. YANG K., LIN D., XING B. Interactions of humic acid with nanosized inorganic oxides. Langmuir. **25** (6), 3571, **2009**.

13. PHILIPPE A., SCHAUMANN G.E. Interactions of dissolved organic matter with natural and engineered inorganic colloids: a review. Environmental science & technology. **48** (16), 8946, **2014**.

14. SCHULZ M., SOLTANI A. Effect of inorganic colloidal water constituents on combined low-pressure membrane fouling with natural organic matter (NOM). Journal of Membrane Science. **507**, 154, **2016**.

15. JERMANN D., PRONK W., BOLLER M. Mutual influences between natural organic matter and inorganic particles and their combined effect on ultrafiltration membrane fouling. Environmental science & technology. **42** (24), 9129, **2008**.

16. LI Q., ELIMELECH M. Synergistic effects in combined fouling of a loose nanofiltration membrane by colloidal materials and natural organic matter. Journal of Membrane Science. **278** (1), 72, **2006**.

17. LIN T., LU Z.J., CHEN W. Interaction mechanisms and predictions on membrane fouling in an ultrafiltration system, using the XDLVO approach. Journal of Membrane Science. **461**, 49, **2014**.

18. LOOSLI F. Effect of electrolyte valency, alginate concentration and pH on engineered TiO_2 nanoparticle stability in aqueous solution. Science of the Total Environment. **535**, 28, **2015**.

19. CHEN L., TIAN Y., CAO C. Interaction energy evaluation of soluble microbial products (SMP) on different membrane surfaces: role of the reconstructed membrane topology. Water research. **46** (8), 2693, **2012**.

20. BRANT J.A., CHILDRESS A.E. Assessing short-range membrane-colloid interactions using surface energetics. Journal of Membrane Science. **203** (1), 257, **2002**.

21. VAN OSS C.J. Acid-base interfacial interactions in aqueous media. Colloids and Surfaces A: Physicochemical and Engineering Aspects. **78**, 1, **1993**.

22. XIAO K., WANG X., HUANG X. Combined effect of membrane and foulant hydrophobicity and surface charge on adsorptive fouling during microfiltration. Journal of Membrane Science. **373** (1), 140, **2011**.

23. SPRINGER F., LABORIE S., GUIGUI C. Removal of SiO_2 nanoparticles from industry wastewaters and subsurface waters by ultrafiltration: investigation of process efficiency, deposit properties and fouling mechanism. Separation and Purification Technology. **108**, 6, **2013**.

24. JERMANN D., PRONK W., KÄGI R. Influence of interactions between NOM and particles on UF fouling mechanisms. Water research. **42** (14), 3870, **2008**.

25. TIAN J., ERNST M., CUI F. Effect of particle size and concentration on the synergistic UF membrane fouling by particles and NOM fractions. Journal of membrane science. **446**, 1, **2013**.